

1 **Remote monitoring of minewater rebound and**
2 **environmental risk using satellite radar**
3 **interferometry**

4
5 David Gee^{1*}, Andrew Sowter¹, Ahmed Athab¹, Stephen Grebby², Zhenming Wu^{1,3}, Kateryna
6 Boiko⁴

7
8 **Affiliations**

9 ¹ Terra Motion Limited, Ingenuity Centre, Triumph Road, Nottingham, NG7 2TU, UK

10 ² Nottingham Geospatial Institute, Faculty of Engineering, University of Nottingham,
11 Nottingham, NG7 2TU, UK

12 ³ Department of Meteorology, University of Reading, Reading, RG6 6BB, UK

13 ⁴ State Ecological Academy of Postgraduate Education and Management, Kyiv, 03035,
14 Ukraine

15
16 *Correspondence to: david.gee@terramotion.co.uk

17
18 **Abstract**

19 The cessation of dewatering following coalfield abandonment results in the rise of
20 minewater, which can create significant changes in the local and regional hydrogeological
21 regime. Monitoring such change is challenging but essential to avoiding detrimental
22 consequences such as groundwater contamination and surface flooding. Inverse modelling
23 methods using satellite radar interferometry (InSAR) have proven capable for retrospectively
24 mapping minewater level changes, however, there is a need for the capability to remotely
25 monitor changes as they occur. In this study, ground deformation measurements obtained
26 from InSAR are used to develop a method to remotely monitor the spatio-temporal rise of
27 minewater, which could be implemented in near real-time. The approach is demonstrated
28 over the Horlivka mining agglomeration, Ukraine, where there is no other feasible approach
29 possible due to a lack of safe ground access. The results were blindly validated against *in-situ*
30 measurements before being used to forecast the time until minewater will reach the natural
31 water table and Earth's surface. The findings reveal that, as a result of military conflict in
32 Donbas, an environmental catastrophe could occur where potentially radioactive minewater is
33 forecast to reach the natural water table between May and August of 2024.

34

35 **Keywords**

36 Coal mining; Minewater rebound; Hydrogeology; Modelling; Surface deformation; InSAR

37

38

39 **1. Introduction**

40 In deep mines that operate below the groundwater table, water is often pumped to the surface
41 to facilitate safe mining, disrupting the natural hydrogeological conditions. When a mine is

42 closed, it is common practice for pumping regimes to partially remain in place to prevent
43 toxic minewater, or acid minewater drainage, from rising rapidly. Such pumping is
44 implemented to avoid groundwater contamination, gas emissions, surface flooding and
45 pollution, soil settlement and subsidence of the surface (Younger, 2016). Obtaining sufficient
46 knowledge of the spatio-temporal rise of minewater is highly desirable to avoid the
47 aforementioned detrimental environmental and socio-economic consequences following the
48 cessation of dewatering. Mine plans and minewater level measurements provide important
49 information with regards to the direction and structural control of groundwater flow.
50 However, information regarding inter-seam connections within collieries, as well as
51 connections between adjacent collieries from mine plans, are often inaccurate or incomplete.
52 In addition, many mine shafts are backfilled after colliery closure and so *in-situ* minewater
53 level measurements often are spatially sparse and drilling new monitoring boreholes is
54 expensive. As a result, only limited information is available to form the basis of remediation
55 strategies in typically vast and complicated mine systems, which have often been extensively
56 worked for decades (Younger & Adams, 1999).

57 A host of modelling methods have been developed in the past decades to quantify and predict
58 the hydrogeological changes that occur following coalfield closure. Ongoing developments of
59 computer hard/software have increased computational capacity. This has facilitated the use of
60 numerical methods to simulate the flow of groundwater through aquifers which have been
61 applied to model the flooding of recently abandoned mines (e.g. Yu *et al.*, 2007; Surinaidu *et*
62 *al.*, 2014). Bespoke simulation packages have subsequently been developed specifically for
63 investigating the flooding of coalfields, including physical-based, spatially distributed models
64 (e.g. Adams & Younger, 1997; Hamm *et al.*, 2008) and simplified semi-distributed models
65 such as Groundwater Rebound in Abandoned Mineworkings (GRAM) (Sherwood &
66 Younger, 1997; Younger & Adams, 1999). GRAM, for example, has been shown to produce

67 useful and realistic results for predicting the time until the hydrogeological conditions return
68 to the pre-mining state. As a different approach, Younger (2016) proposed an alternative to
69 computer-based simulations by using rudimentary calculations based on information such as
70 voidage, water inflow rates and topography.

71 Changes in groundwater levels can cause the Earth's surface to rise and fall, which can be
72 measured remotely using satellite radar interferometry (InSAR) (Hoffmann *et al.*, 2001).
73 InSAR is an Earth observation technique which is capable of measuring millimetric rates of
74 ground deformation from the differences in phase between radar images. Such data provide
75 the means to calibrate groundwater models, delineate lithological boundaries, map aquifer
76 storage variations and assist aquifer characterization (e.g. Boni *et al.*, 2016; Castellazzi *et al.*,
77 2016; Béjar-Pizarro *et al.*, 2017). InSAR has become a standard technique for surface motion
78 measurement (Crosetto *et al.*, 2020) and, advantageously, can be utilized to generate
79 historical, present and future ground deformation measurements in inaccessible areas around
80 the world. This capability has been greatly enhanced since 2014 by the free, open-access and
81 global data supplied by the Sentinel-1 mission (Torres *et al.*, 2012). Furthermore, novel
82 processing methods such as the APSIS (Advanced Pixel System using Intermittent SBAS)
83 (Sowter *et al.*, 2013; Sowter *et al.*, 2016) InSAR method are able to significantly extend the
84 coverage of conventional techniques – such as persistent scatterers interferometry (PSI) and
85 the small baseline subset (SBAS) method – to provide a near 100% coverage of
86 measurements over urban and rural areas alike. This is vital for InSAR inversion approaches,
87 since the response of the subsurface to pressure changes associated with variations in
88 groundwater can be highly spatially variable due to differences in the compressibility,
89 thickness and confinement of the strata (Castellazzi *et al.*, 2018).

90 With the increased availability of InSAR data, numerical methods have more recently been
91 developed and applied to determine the surface deformation associated with minewater

92 rebound (e.g. Todd *et al.*, 2019; Dudek *et al.*, 2020; Zhao & Konietzky, 2020). In this regard,
93 numerical approaches have proven to be valuable for effectively simulating minewater rise in
94 complex geologies and mining conditions. Moreover, they also have the potential to provide
95 more comprehensive information than just surface displacements, such as strain, stress and
96 fracture patterns (Zhao & Konietzky, 2021). However, numerical approaches require detailed
97 mining information, are typically difficult and time-consuming to set-up, and are often too
98 complex to implement at the coalfield scale. Alternatively, analytical approaches are much
99 easier to set-up, can be implemented over vast areas and use relatively simple calculations,
100 hence, crucially, they are well suited to solve inverse problems (i.e. inference of minewater
101 levels from surface deformation data). Temporal correlations between the rise of minewater
102 and InSAR measurements have been recognized (e.g. Samsonov *et al.*, 2013; Gee *et al.*,
103 2017; Malinowska *et al.*, 2020) and such measurements have been used in inversion
104 approaches to retrospectively map minewater changes in recently abandoned coalfields (e.g.
105 Cuenca *et al.*, 2013; Gee *et al.*, 2020). However, there is still a lack of approaches for
106 monitoring changes in minewater levels across entire coalfields as they occur.

107 Monitoring such change is challenging yet essential to avoiding the potential detrimental
108 environmental impacts of minewater rebound. This is because access to detailed and up-to-
109 date information could be used to help identify when and where appropriate mitigation
110 measures need to be put in place. Accordingly, the aim of this study is to present a method for
111 near real-time remote monitoring of minewater levels across an entire abandoned coalfield,
112 for the purpose of determining the potential environmental risk. Pertinently, this is
113 demonstrated over the Horlivka mining agglomeration, Donbas, Ukraine, where there is no
114 other feasible monitoring approach due to a lack of safe ground access and intermittent *in-situ*
115 measurements owing to the military conflict between Ukraine and Russia. The specific
116 objectives are to:

- 117 (i) generate and calibrate a model to establish the relationship between the change in
118 minewater levels and surface deformation;
- 119 (ii) remotely monitor the change in minewater levels using InSAR and blindly
120 validate against the available *in-situ* measurements;
- 121 (iii) forecast the time it will take for minewater to reach the natural water table and
122 Earth's surface;
- 123 (iv) discuss the environmental implications of abrupt mine closure in Donbas.

124 The remainder of the manuscript is structured as follows. The study site and materials are
125 introduced in section two providing the geological and hydrogeological context for the study.
126 Objectives i-iii provide the structural sub-headings for the methodology and results and
127 discussion in sections three and four, respectively. A discussion is provided in section five to
128 addresses objective four before a conclusion in section six.

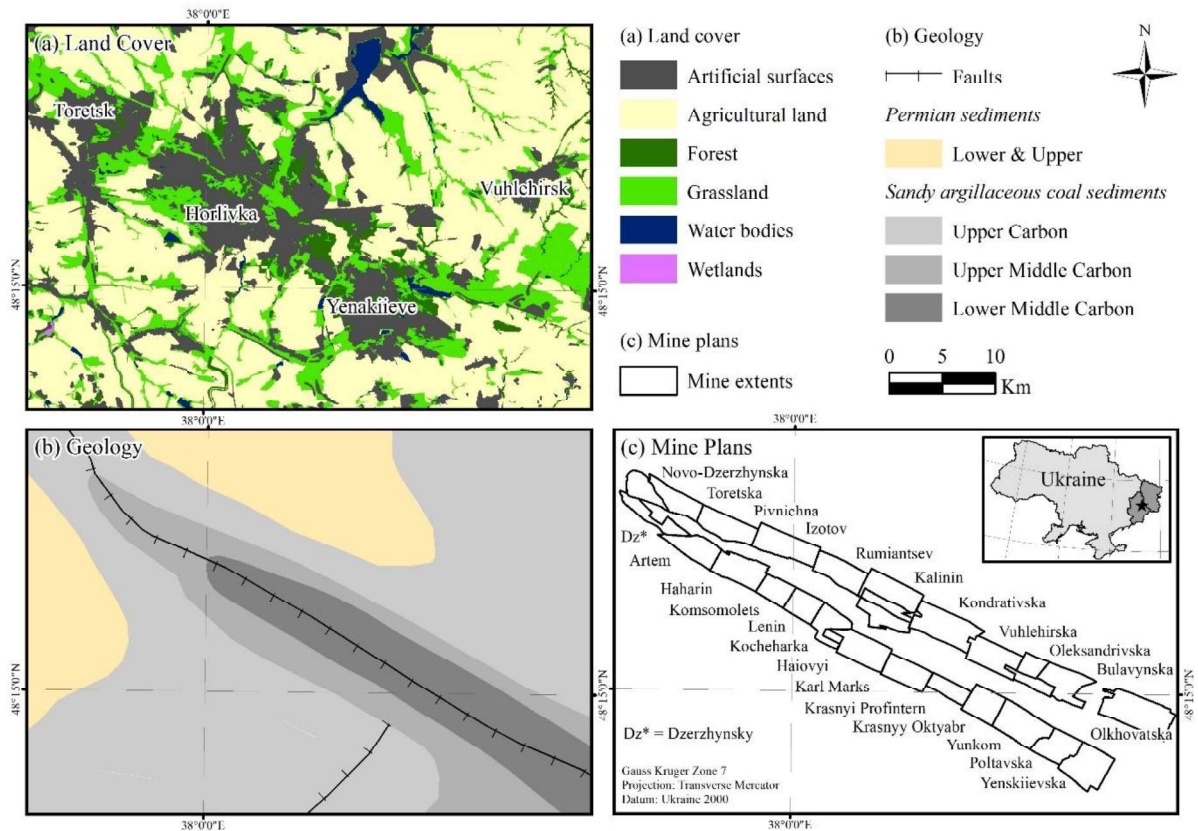
129

130 **2. Study site & materials**

131 **2.1 Land cover**

132 The study site is approximately 40 x 50 km and is located in the north-east of the Donetsk
133 oblast, Ukraine (Fig. 1). Artificial surfaces make up 19% of the area which predominantly
134 correspond to the cities of Toretsk, Horlivka and Yenakiieve which orientate from WNW-
135 ESE. The remainder of the land cover is rural, dominated by agricultural land (59%) as well
136 grasslands (16%), forest (4%) and wetlands (<1%) (Chen *et al.*, 2015). Water bodies
137 comprise the remaining two percent.

138



140 **Figure 1.** Horlivka mining agglomeration: (a) Land cover (Chen *et al.*, 2015); (b) geology; (c) mine plans.

141

142 **2.2 Geology**

143 The Horlivka mining agglomeration is situated within the Donets Basin (colloquially referred
 144 to as Donbas), which is one of the world’s major Late Palaeozoic coalfields with proven
 145 reserves of ~60 Gt (Alsaab *et al.*, 2009). The Donets Basin forms the south-eastern part of the
 146 Dniepr-Donets Basin, which is a Late Devonian rift structure on the southern part of the
 147 Eastern European craton (Stovba & Stephenson, 1991). The Donets Basin fill comprises
 148 Devonian pre- and syn-rift rocks and a complete Carboniferous-Palaeogene post-rift sequence
 149 several thousands of metres thick (Sachsenhofer *et al.*, 2002). A major part of the basin, the
 150 Donbas Foldbelt, has been inverted and is characterized by a series of WNW–ESE-trending
 151 folds and faults. The most dominant of these structures is the Gorlovka (Horlivka) Anticline,

152 which is a near-symmetrical structure with steeply dipping limbs of 60-80°, bordered by the
153 Main (north) and South synclines and North and South Anticlines (Sachsenhofer *et al.*, 2002).
154 There are more than 300 coal layers contained to within a depth of 1800 m of the
155 Carboniferous fill of the Donets Basin, of which approximately 130 are considered to be
156 workable coal seams due to their thickness (i.e. >0.45 m) and depth constraints (Alsaab *et al.*,
157 2009). Coal mines in the region have operated at depths of 220–1380 m, with an average
158 depth of 620 m (Privalov *et al.*, 2003). Coals within the Donets Basin have high ash yields
159 (12–18%), high sulphur contents (2.5–3.5%) and are rich in hazardous trace elements such as
160 Hg, As, Cd, Pb and Zn, with particularly high concentrations of Hg found along the Gorlovka
161 anticline (Sachsenhofer *et al.*, 2012), where the Horlivka mining agglomeration is located. In
162 this study, the Horlivka mines are grouped into the northern and southern agglomeration
163 according to their location on the northern and southern limbs of the Gorlovka anticline,
164 respectively (Fig. 1). A measurement of the (initial) porosity is required for the establishment
165 of the minewater model and, in the absence of laboratory samples, a measurement of 0.15
166 was defined in accordance with Donabedov (1940).

167

168 **2.3 Hydrogeology**

169 The eastern Ukrainian oblasts of Donetsk and Luhansk have been subject to conflict between
170 the Ukraine military and Russian-backed separatists since 2014. The ecology in eastern
171 Ukraine was in a fragile state prior to the hostilities and is worsening over time as the quality
172 of water and soils are being degraded by the mass and abrupt closure of over 30 deep coal
173 mines in the region. Many of pumping systems have been switched off, damaged or subject
174 to power cuts and, consequently, the rise of minewater risks contamination of the region's
175 soils, groundwater and surface waters (Hook & Marcantonio, 2022). The uppermost

176 geological zone of the agglomeration is subject to high levels of chemical contamination and
177 over 4000 ecologically hazardous facilities have been identified, including metallurgical and
178 chemical enterprises, sludge depositories and waste ponds, which include the Horlivka
179 Chemical Plant, Mykytivskiy mercury mine and the Yunkom coal mine (Ministry of Ecology
180 and Natural Resources of Ukraine, 2019; Yermakov *et al.*, 2019). Many mines have been
181 operating for 50-70 years and there is a significant quantity of steeply dipping coal seams
182 (over 55°). Due to mining operations, anthropogenic cracking has increased permeability and
183 developed new routes for the accelerated migration of contaminants and interconnection
184 between ground and surface waters. This has reduced the protective ability of the uppermost
185 zone of the geological system. At present, practically all of the mines within the Horlivka
186 urban mining agglomeration, on the northern and southern flanks of the anticline, are
187 hydraulically interconnected at depths that range from 230–1080 m, creating a unitary system
188 with high anthropic groundwater vulnerability (Chumachenko & Yakovliev, 2017).

189 Minewater depth measurements were supplied by State Ecological Academy of Postgraduate
190 Education and Management, Ukraine. The measurements were obtained manually from the
191 mine shafts because the monitoring network is no longer operational. The levels, acquired at
192 monthly intervals, were made available to the modelers for 19 mines in the Horlivka mining
193 agglomeration and cover nearly a two-year period from 1st November 2017 to 1st September
194 2019. Once the modelling had been conducted, the depths in the February 2022 were supplied
195 for validation. There were less validation measurements available, ten, owing to the lack of
196 safe ground access.

197

198 **2.4 Earth observation data**

199 Two hundred and seventy-eight Sentinel-1 Level-1 Interferometric Wide (IW) Single Look
200 Complex C-Band radar images covering the period 5th March 2015 to 20th February 2022
201 were available over the Horlivka mining agglomeration. The images were acquired on a
202 descending orbit from track 94 and have a medium revisit time of 6 days. The incidence
203 angle at Horlivka is $\sim 37^\circ$ and the IW products have a pixel spacing of 2.3 m in slant range
204 and 13.9 m in azimuth, corresponding to a spatial resolution 5 m in ground range and 20 m in
205 azimuth at scene centre (Torres *et al.*, 2012). There is insufficient data covering a similar time
206 epoch from an ascending track making a stereo analysis unfeasible.

207

208 **3. Monitoring methodology**

209 **3.1. Generation & calibration of minewater model**

210 **3.1.1. Forward minewater model**

211 An analytical model was established to ascertain the relationship between the change in
212 minewater levels and surface deformation (and vice-versa). Using basic correlations that
213 universally determine a value of groundwater rise per unit of surface deformation lead to
214 erroneous interpretations because minewater rising closer to the surface has a stronger effect
215 on surface deformation than rising minewater at depth. Similarly, minewater rise in an
216 unconfined aquifer results in more surface deformation than a rise within coal measures that
217 are confined by overlying strata (Gee *et al.*, 2020). The forward model is based upon the
218 principle of effective stress (Terzaghi, 1925; Poland, 1984) and calculates the increase or
219 decrease in the thickness of the strata (i.e. heave or subsidence) for a given change in
220 minewater levels, in accordance with Gee *et al.* (2020). The model is treated as a
221 homogeneous matrix, where the initial bed thickness (b_0) (m) was calculated as the depth
222 from the surface to the minewater level at the start of the modelling epoch, for each

223 individual mine. The strata is subject to a level of geostatic pressure (p) (kPa), which
224 increases as more material is overlain over time. Geostatic pressure is resisted by the
225 intergranular (effective) stress (p_{s0}) of the rock matrix and the fluid pressure of pore water
226 (p_{w0}) (Poland, 1984) such that:

$$227 \quad p = p_{s0} + p_{w0} \quad (\text{Eqn. 1})$$

228 Equilibrium must be maintained in Eqn. 1, thus, an increase in minewater increases the pore
229 fluid pressure and decreases the effective stress on the strata. This causes an expansion of the
230 strata until equilibrium is again reached. The geostatic pressure (p) was calculated from the
231 initial bed thickness (b_0) using 10 kPa/m to calculate the stress transfer from fluid to rock
232 matrix per unit change in minewater levels (Poland, 1984) as:

$$233 \quad p = 10 \cdot b_0 \quad (\text{Eqn. 2})$$

234 The entire coalfield is exposed (i.e. there is no overlying strata) and therefore it is treated as
235 an unconfined aquifer where geostatic pressure is attributed as 65% effective stress and 35%
236 pore fluid pressure. Following the change in minewater levels (Δh), the new pore fluid
237 pressure (p_w) is calculated as:

$$238 \quad p_w = p_{w0} + 10 \cdot \Delta h \quad (\text{Eqn.}$$

239 3)

240 and by maintaining the equilibrium in Eqn. 1, the new effective stress (p_s) is:

$$241 \quad p_s = p - p_w \quad (\text{Eqn.}$$

242 4)

243 Hence, the change in effective stress (Δp_s) can be expressed as a function of the initial
244 geostatic pressure (Eqn. 1) and change in minewater where:

$$245 \quad \Delta p_s = p_s - p_{s0}$$

$$\begin{aligned}
246 \quad &= p - p_w - p_{s0} \\
247 \quad &= p - p_{w0} - 10 \cdot \Delta h - p_{s0} \quad (\text{Eqn. 5})
\end{aligned}$$

248 The initial void ratio (e_0) is calculated from the initial porosity (n_0) by:

$$249 \quad e_0 = \frac{n_0}{1 - n_0} \quad (\text{Eqn. 6})$$

250 and after a change in effective stress a new void ratio (e) is calculated as:

$$251 \quad e = e_0 - c_c \cdot \log\left(\frac{p_s}{p_{s0}}\right) \quad (\text{Eqn. 7})$$

252 expressed as a function of the initial void ratio (e_0), the compression index (c_c) and the initial
253 (p_{s0}) and new effective stress (p_s). The compression index is a dimensionless parameter that
254 determines the compressibility of the stratigraphic bed and considers the elastic properties of
255 the unit. For each mine, the InSAR data were used to determine the compression index and
256 calibrate the model, as outlined in sub-section 3.1.2.

257 The coefficient of volume compressibility (m_v) relates the coefficient of compressibility (a_v)
258 and the initial void ratio (e_0) as:

$$259 \quad m_v = \frac{a_v}{1 + e_0} \quad (\text{Eqn. 8})$$

260 where,

$$261 \quad a_v = \frac{\Delta e}{\Delta p_s} \quad (\text{Eqn. 9})$$

262 and Δe is the difference in void ratio.

263 The change in bed thickness (Δb) is caused by the change in effective stress (Δp_s), and is
264 calculated as a function of the coefficient of volume compressibility (m_v) and the initial
265 thickness of the unit (b_0) by:

266 $\Delta b = \Delta p_s \cdot m_v \cdot b_0$ (Eqn. 10)

267

268

269 **3.1.2. Model calibration & inversion**

270 Surface deformation measurements are required to calibrate the model and provide
271 measurements for inversion. The Sentinel-1 data were processed using the APSIS InSAR
272 method (Sowter *et al.*, 2013; Sowter *et al.*, 2016). The APSIS algorithm was used due to the
273 dominance of rural land cover, since it has been shown to be capable of returning a set of
274 dense measurements over almost every land cover type over wide areas (e.g. Sowter *et al.*,
275 2018; Gee *et al.*, 2019). This is vital given that 91% of land cover is rural within Donetsk and
276 Luhansk (Chen *et al.*, 2015). Importantly, unlike conventional InSAR techniques, APSIS can
277 provide such coverage without the installation of ground infrastructure or recourse to ground
278 survey, both of which are currently unfeasible in Donbas due to the inaccessibility of the
279 region during the conflict.

280 Once the image stack was co-registered, 3243 small-baseline interferograms were generated
281 between pairs with a maximum temporal baseline of 365 days and a maximum perpendicular
282 baseline of 30 m. Topographic phase was simulated and removed using a 90 m digital
283 elevation model from the TanDEM-X mission (German Aerospace Center, 2018), and
284 interferograms were multi-looked by a factor of 7 in range and 2 in azimuth. Unwrapping was
285 performed using a modified version of the SNAPHU algorithm. The average rate of motion
286 and time-series were calculated for pixels at a resolution of 20 m using linear and non-linear
287 models of deformation, respectively. The measurements were projected from the satellite
288 line-of-sight into the vertical by means of dividing by the cosine of the incidence angle.

289 Finally, to reduce the effect of noise in the model the time-series were spatially averaged over
290 a 1 km window.

291 The model was calibrated over the period for which *in-situ* minewater level measurements
292 were available (1st November 2017–1st September 2019). The difference in the relative
293 heights of the time-series over this period was calculated, with the time-series being linearly
294 interpolated to the latter date given that no image and, hence, no time-series measurement
295 was available for this date. The compression indices that minimized the root-mean-square-
296 error between the forward model at the mine shaft location and 99th percentile of the InSAR
297 time-series difference within the mine extent were calculated for each mine. Once suitably
298 calibrated, the forward model was implemented across the coalfield. Finally, the InSAR time-
299 series difference was utilized as the measure of the change in bed thickness (Δb), which was
300 inverted to quantitatively map the change in minewater levels (Δh) across the coal district
301 over the calibration period (2017–2019), as given by:

$$302 \quad \Delta h = \frac{1}{10} (p - p_{so} - p_{wo} - \left(\frac{\Delta b}{m_v b_0}\right)) \quad (\text{Eqn. 11})$$

303

304

305 **3.2. Remote monitoring of minewater rise**

306 The recovery of minewater is not a linear process as the rate of rebound decreases
307 exponentially over time, as minewater approaches the surface (Younger & Adams, 1999).
308 The relationship between the compression indices and groundwater depths for each of the
309 mines over the calibration epoch were analyzed to determine the reduction of inflow with
310 depth. As minewater gets closer to the surface the compression index decreases; a logarithmic
311 fit between the compression index and minewater depth was established producing a

312 coefficient of determination (R^2) of 0.77. To estimate the minewater rise for the remaining
313 portion of the time-series, the model was run iteratively. The time-series were offset to the
314 end of the calibration period (1st September 2019) and the first relative height change of the
315 remaining portion of time-series was inverted to retrieve the change in minewater levels (Δh)
316 (Eqn. 11). This results in a new minewater depth, and a new compression index was retrieved
317 utilizing the function between the compression index and minewater depth. The forward
318 model was re-generated to determine the change in bed thickness (Δb) using the newly
319 inverted change in minewater depth and new compression index (Eqns. 1–10). This was
320 repeated for the remainder of the time-series. The iterative model was developed and
321 implemented blind of the *in-situ* minewater measurements over the period 2019–2022.

322

323

324 **3.3. Forecasts of minewater rise**

325 A linear trendline, with \pm one standard deviation of the linear regression, was fitted to the
326 inverted minewater depths and used to forecast the time interval until the minewater will
327 reach the water table and Earth's surface. In Donbas, the natural water tables lies between
328 20–70 m below the surface so a conservative value of 70 m was utilized (State Ecological
329 Academy of Postgraduate Education and Management of the Ministry of Ecology and
330 Natural Resources of Ukraine, 2018). Linear projections are often used by managing
331 authorities as they provide an estimate towards the worst case. This is preferable to an
332 exponential fit which might erroneously indicate an area is not at risk.

333

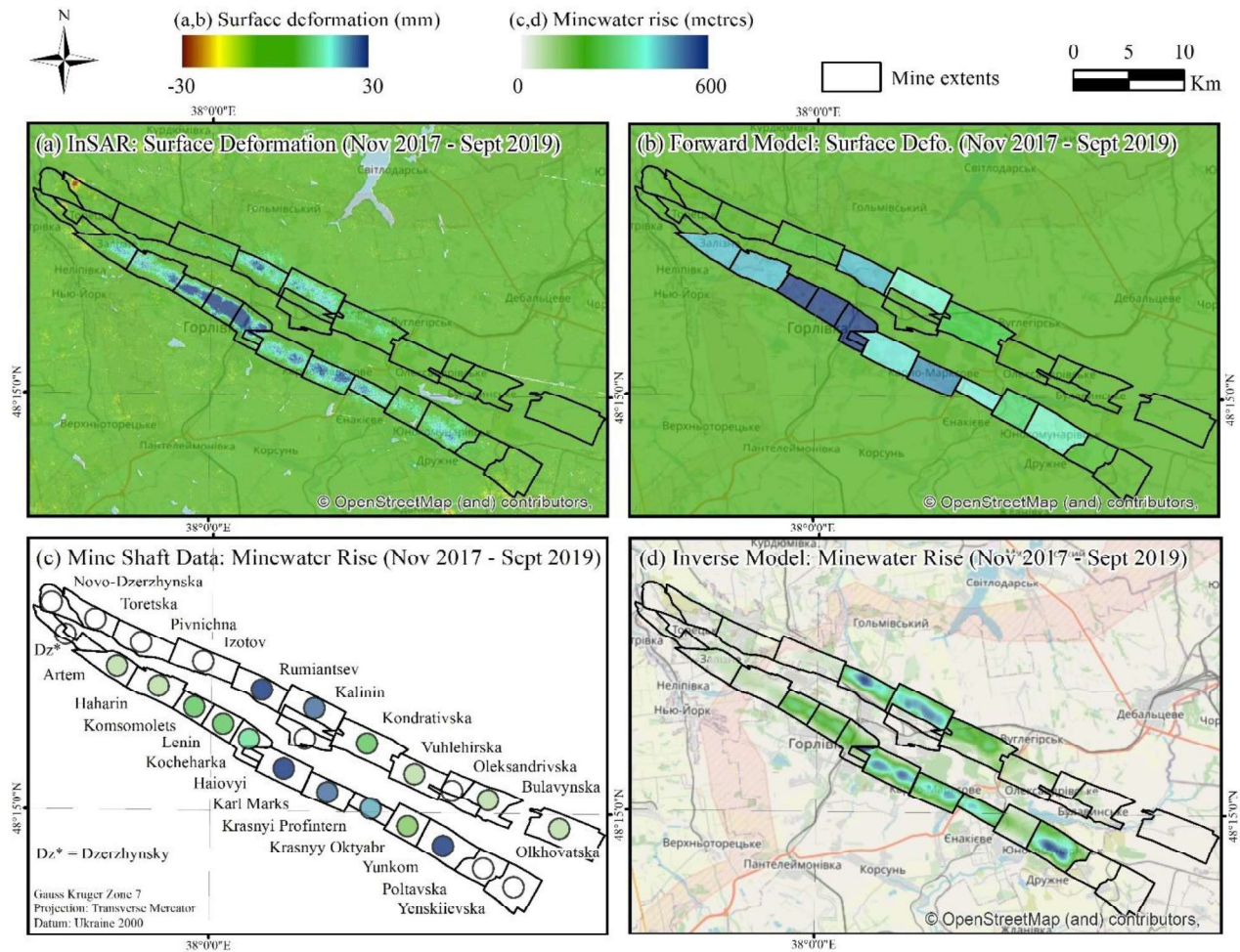
334

335 4. Results and discussion

336 4.1. Generation & calibration of minewater model

337 The forward model estimates the surface deformation caused by the change in minewater
338 levels as measured within the mine shafts and good agreement between InSAR and modelled
339 heave is found (i.e. heave occurs over mines where minewater is rebounding) (Fig. 2a,b).
340 This confirms that heave observed at the surface above the mines is due to minewater
341 rebound. The coal measures rock are subject to a level of geostatic pressure which is resisted
342 by the rock matrix and the pore space within the rock. As the mines flood, the pore fluid
343 pressure increases causing expansion of the strata which manifests as heave at the surface
344 (Bekendam & Pöttgens, 1995; Poland, 1984). The forward model represents a simplification
345 of the rebound occurring as a single measurement from within the mine shaft is used for the
346 entire mine extents and the boundaries of which may not be wholly accurate. The InSAR
347 measurements capture the variability in minewater rise which, when inverted, provides a
348 detailed characterization of the rise in minewater. The inverted InSAR measurements assume
349 that heave occurs solely as a result of rising minewater, which may not always be the only
350 cause of the observed ground motions. However, it is a reasonable assumption given that the
351 spatially correlated heave is delimited by the structural geology and has been validated by
352 the forward model. The inverted measurements demonstrate good agreement with the *in-situ*
353 minewater measurements over the calibration period (November 2017–September 2019) (Fig.
354 2c,d). The inverted measurements account for the depth of minewater and, for example,
355 correctly determine that minewater rose over twice as fast at Yunkom (612 m) than at Lenin
356 (291 m) despite surface heave measuring four times less at Yunkom, ~15 mm compared to
357 ~60 mm at Lenin.

358



360

361 **Figure 2.** Surface deformation and minewater rise over the initial calibration period (1st of November 2017-1st
 362 September 2019) at the Horlivka mining agglomeration: (a) InSAR surface height change; (b) surface height
 363 change estimated by the calibrated forward model; (c) changes in minewater levels as measured within the mine
 364 shafts; (d) change in groundwater levels as derived from the inverse model.

365

366

367 **4.2. Remote monitoring of minewater rise**

368 The cross-sections through the northern and southern group of mines show the depth of
 369 minewater above mean sea level (a.m.s.l) as measured from *in-situ* data in November 2017

370 and September 2019, and the modelled levels in February 2022 (Fig. 3). The total change in
371 minewater levels over September 2019 – February 2022 is shown in Fig. 4 and Fig. S1,
372 which demonstrate good agreement with the *in-situ* data, where available. Making a direct
373 quantitative comparison between the two datasets is challenging since the shaft
374 measurements are of a single point, whereas the modelled data provides measurements over
375 the entire mine complex. The effects of rebound can often be highly spatially variable, even
376 within a single mine, and the most prominent areas of rebound can occur away from the shaft.
377 For instance, a mine might have a small concentric area of rebound (e.g. Haiovy) or a
378 broader area covering the entire mine extents (e.g. Kalinin). Consequently, determining an
379 evaluation metric, such as the mean within 500 m of the shaft or the median of all pixels
380 within the mine extents, to compare against the *in-situ* data that appropriately reflects the
381 models capability is challenging because the most appropriate and representative metric can
382 change from mine to mine. One of the benefits of using this satellite based method is that
383 measurements are provided across the entire mine extents and not just of a single point.
384 Furthermore, it does not require detailed mine plans, hydraulic connections or fault
385 information to achieve this. Advantageously, the presence of such features can be detected by
386 the model. For example, if a connection to a neighbouring mine is reached uplift and the
387 modelled minewater levels will begin to plateau. As minewater decants into the neighbouring
388 mine, heave will likely start to be detected by the InSAR data and, therefore, rising
389 minewater levels will be observed by the model.

390 Rebound is greater over the period from 2017–2019 than over 2019–2022, which is because
391 the recovery of minewater is not a linear process, whereby the rate of rebound exponentially
392 slows as the minewater approaches the surface. This occurs because the groundwater head
393 difference between the recovering mined areas and the surround strata reduces with recovery
394 and, hence, so does the rate of inflow into the recovering areas. Additionally collapsed

395 shallow workings act to increase effective permeability closer to the surface and as
396 minewater reaches shallower depths it interacts with the broader hydrogeological cycle (i.e.
397 inflows and outflows into the river network) (Younger & Adams, 1999).

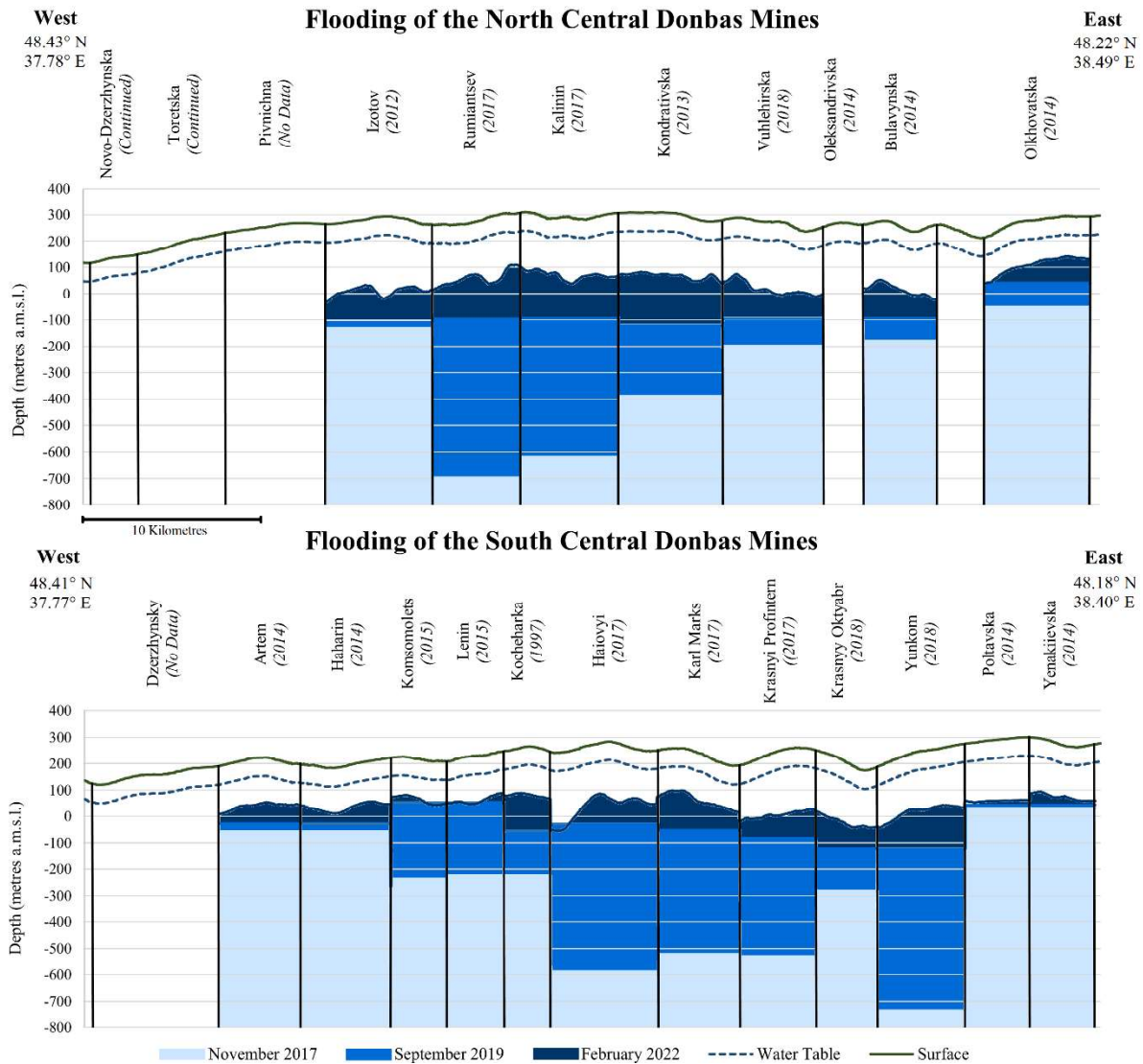
398 Within the string of mines in the north, pumping continues in Novo-Dzerzhynska and
399 Toretska, while no data is available for the Pivnichna mine. Pumping ceased within
400 Rumiantsev and Kalinin in 2017, which has resulted in minewater rising from depths of -600
401 m – -700 m a.m.s.l to -100 m, which is characterized in the inverted minewater rates over the
402 calibration period (Fig. 1d). The cessation of pumping in these two mines has likely caused
403 levels in the adjacent Kondrativska mine to rise (where pumping ceased in 2013), given that
404 known connections are present between the mines at these depths (Ministry of Ecology and
405 Natural Resources of Ukraine, 2019). Further east, with the exception of Vuhlehirska where
406 pumping ceased in 2018, the Oleksandrivska, Bulavynska and Olkhovatska mines ceased
407 pumping in 2014 and as a result minewater depths are closer to the surface than the mines
408 further west. No data is available in the Oleksandrivska mine, however, given that the
409 adjoining Vuhlehirska and Bulavynska mines have near identical minewater levels in 2017,
410 2019 and 2022 and that a connection between all three mines exists at -260m a.m.s.l.
411 (Ministry of Ecology & Natural Resources of Ukraine, 2019), it could be inferred that levels
412 here are similar.

413 The characteristics of rebound within the southern agglomeration of mines can approximately
414 be characterized into three areas. Pumping ceased prior to 2015 in the west (consisting of the
415 Artem, Haharin, Komsomolets, Lenin and Kocheharka mines), and by 2019 levels are
416 approximately between $\sim \pm 50$ m a.m.s.l. Whilst minewater continues to rise at Artem and
417 Haharin in 2022, the Komsomolets and Lenin minewater levels have plateaued and/or fallen.
418 At this depth minewater can be prone to seasonal changes (Fig 3; 5a). In the central area,
419 consisting of Haiovyι, Karl Marks, Krasnyi Profintern, Krasnyy Oktyabr and Yunkom,

420 pumping ceased later (in 2017 or 2018) and, consequently, minewater instantly rose rapidly –
421 over 600 m over two years in the case of Yunkom. Since 2019, rates of rebound have slowed
422 as the minewater levels approach the surface but are still rising in 2022. The Poltavaska and
423 Yenakiievska mines are furthest east and are isolated from those to the west (Ministry of
424 Ecology & Natural Resources of Ukraine, 2019). Here, pumping ceased in 2014 and levels
425 have remained relatively stable since 2017. A connection exists between Yunkom and
426 Poltavaska at ~ 70 m a.m.s.l. and the inverted levels within Yunkom in February 2022 predict
427 that minewater is close to reaching this connection, hence, facilitating the mixing of
428 minewaters between these groups of mines.

429

430



431

432

Figure 3. Minewater depths in 2017 (mine shaft measurements), 2019 (mine shaft measurements) and 2022

433

(inverted InSAR depths) for the northern and southern groups of the Horlivka mining agglomeration. The two

434

transects where the inverted InSAR depths have been extracted are marked on Figure 4a. The horizontal black

435

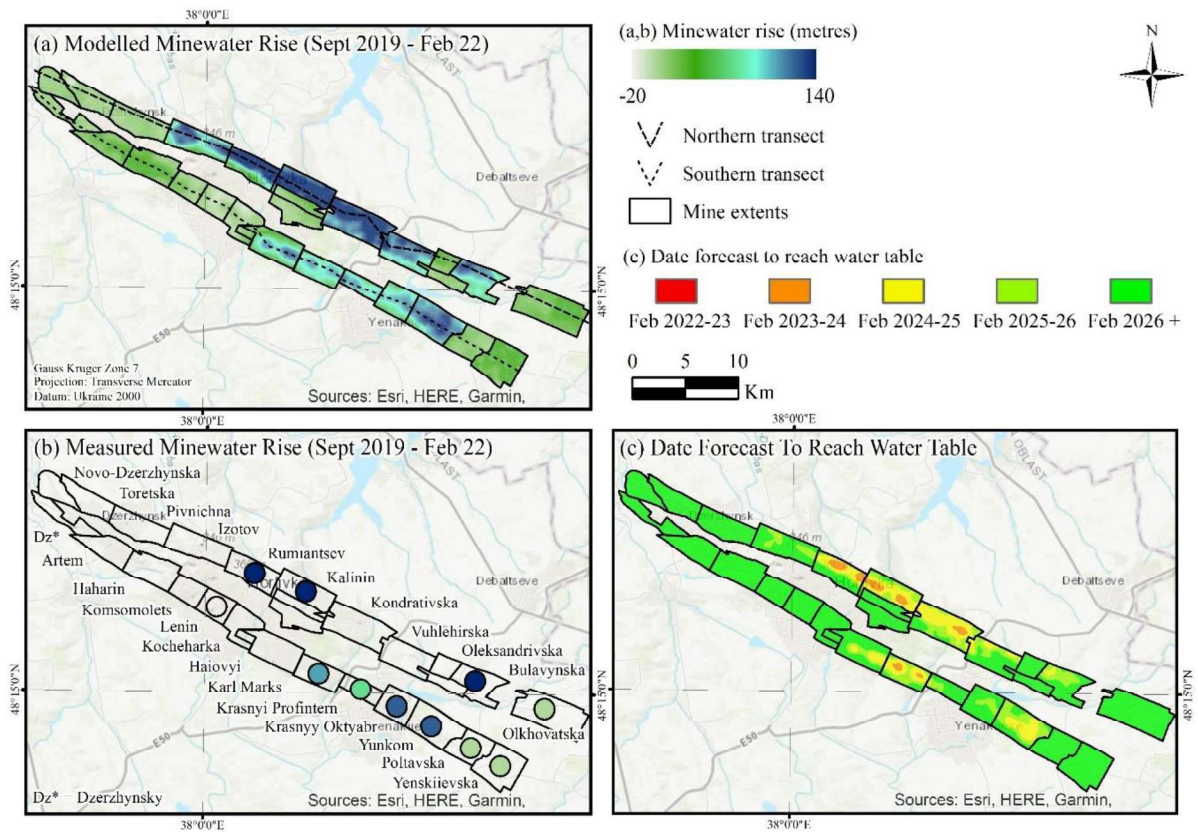
lines demark the mine boundaries. The date that pumping ceased is detailed below the mine labels (Ministry of

436

Ecology & Natural Resources of Ukraine, 2019).

437

438



439

440 **Figure 4.** Minewater rise and forecasts: (a) Modelled change in minewater depth (September 2019 – February
 441 2022); (b) actual change in minewater depth as measured in the mine shafts (September 2019 – February 2022);
 442 (c) estimated time until minewater will reach the water table.

443

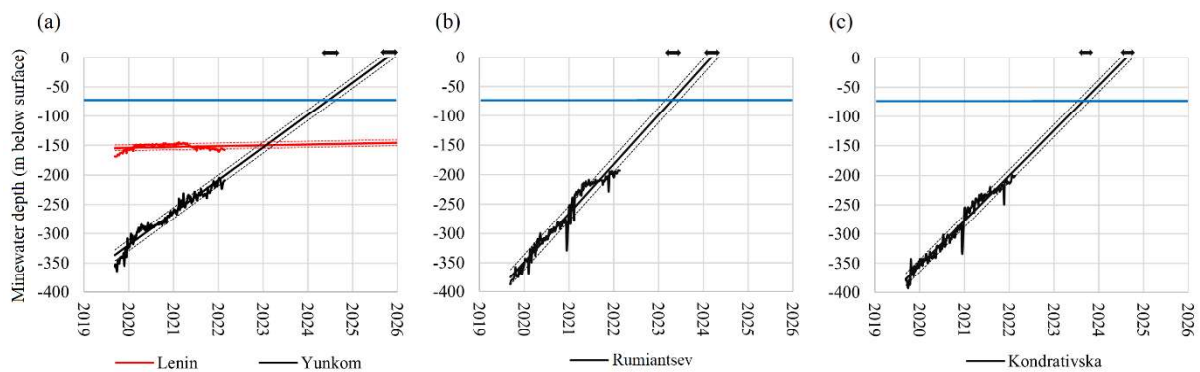
444

445 4.3. Forecasts of minewater rise

446 The projected time at which minewater will take to reach the water table is shown in Fig 4c
 447 and selected time-series are shown in Fig. 5. The projections are indicative of the area’s most
 448 at risk and assume that the minewater regime of the remotely monitored period continues
 449 (2019-22) which might not be the case. For instance, rates could increase if pumping is
 450 reduced or if a seam interval of relatively low yield rapidly floods. Alternatively, rates could
 451 decrease if an extensively worked seam of relatively high specific yield floods or if a
 452 connection to a neighbouring mine is reached. Nevertheless, it is indicative of when and

453 where minewater discharges will occur based upon the latest measurements, which could be
 454 regularly updated in the implementation of a monitoring scheme. Within the coalfield, the
 455 Rumiantsev mine is forecast to reach groundwaters first, in Spring 2023, albeit towards the
 456 end of the time-series there is some evidence that the rate of rebound is reducing and levels
 457 appear that they could stabilize in the future. In the neighbouring mines of Kalinin,
 458 Kondrativska and Vuhlehirska, the minewater is predicted to reach the water table in the
 459 second half of 2023 and early 2024. In the west of the southern agglomeration (Artem to
 460 Kocheharka), rates have slowed significantly or are declining as in the case of Lenin, for
 461 example. In the east within Yunkom, minewater is predicted to reach groundwaters by the
 462 middle of 2024 and there is no evidence that the rate of rebound is decreasing as of February
 463 2022.

464



465

466 **Figure 5.** Time-series of minewater rise and forward forecast: (a) Lenin and Yunkom (forecast to reach the
 467 water table between 3rd May 2024 & 31st August 2024 and the surface between 8th July 2025 & 6th December
 468 2025); (b) Rumiantsev (forecast to reach the water table between 22nd March 2023 & 12th June 2023 and the
 469 surface between 23rd January 2024 & 14th May 2024); (c) Kondrativska (forecast to reach the water table
 470 between 25th June 2023 & 1st November 2023 and the surface between 22nd June 2024 & 29th September 2024).
 471 The dashed lines show \pm one standard deviation of the linear regression and the blue horizontal lines 70 m
 472 below the surface demarks the water table.

473

474

475

476 **5. Environmental implications for Donbas**

477 It is only relatively recently that attention has been brought to the environmental
478 consequences of military conflicts (Ulytsky *et al.*, 2018). Donbas hosts one of the world's
479 largest coal-mining technogenic geosystems with a high density of potentially hazardous
480 facilities (Yermakov *et al.*, 2019). The neglect of pumping by the occupying administrations
481 poses a serious risk of uncontrolled flooding and the leakage of toxic and/or radioactive
482 substances (Yakovliev & Chumachenko, 2017; Yakovliev *et al.*, 2020). Access to the Donbas
483 mines by scientists and Ukrainian authorities has become more and more limited and there is
484 now insufficient and incomplete information about the state of the geological environment
485 and mining space in a majority of mines or hydraulically connected groups of mines
486 (Yakovliev & Chumachenko, 2017; Ulytsky *et al.*, 2018; Sadavenko *et al.*, 2020). The
487 Ministry of Ecology and Natural Resources of Ukraine (2019) concluded it was essential that
488 the monitoring network of boreholes be upgraded and modernized to provide complete and
489 up-to-date data on the status of the groundwater, the geodynamic status of the rock mass and
490 the chemical and ecological status of the surrounding environment. However, on 24th
491 February 2022 Russia launched a full-scale invasion of Ukraine and this is likely to make the
492 remediation of rising minewater in Donbas even less of a priority and therefore highly
493 challenging.

494 The remotely identified changes in minewater levels and the forecasts of rebound are notable.
495 Chumachenko & Yakovliev (2017) concluded that, should the mines in the Horlivka
496 agglomeration become partially or fully flooded without engineered safeguards to isolate and
497 protect the waterproofing of waste-storage facilities, the arrival of contaminated materials

498 into the mines, aquifers and surface waters will likely prove disastrous. Whilst the exact
499 outcomes are hard to predict, consequences are likely to include: surface deformations which
500 might result in damage to the foundations of ecologically hazardous facilities such as toxic
501 waste ponds and oil pipelines; a risk of atmospheric contamination from mine workings and
502 other facilities with highly toxic unstable compounds in liquid or gaseous forms; long term
503 migration of anthropic contaminants into ground and surface waters that are used for
504 domestic water supply; and entry of toxic compounds into the food chain due to the flooding
505 of agricultural areas (Chumachenko & Yakovliev, 2017; Ulytsky *et al.*, 2018). There is
506 already evidence of surface waters becoming polluted with minewater in the surrounds of
507 Horlivka and Yenakiieve (Eastern Option, 2020).

508 It is not fully understood what levels of pumping and management are undertaken in mines
509 outside of Ukrainian control. Within the Horlivka mining agglomeration, according to
510 unofficial information, the occupying authorities may still pump at so-call buffer mines,
511 suggested to be Kalin, Lenin, Karl Marks, Yenakievksa and Olhovatska. However, the
512 projected time until minewater reaches the natural water table within the Yunkom mine, mid
513 2024, is alarming. In 1979, an industrial underground nuclear explosion was undertaken
514 within the mine to assess its effectiveness for reducing the occurrence of sudden gas and coal
515 outbursts (Sadavenko *et al.*, 2020). The radioactive remnants of explosion chamber, the
516 Klivazh facility, remain at approximately 900 m below the surface and Yakovliev *et al.*
517 (2020) note that insufficient technological and physical remediation measures have been
518 implemented in concurrence with the abandonment of the mines of the central mining district.
519 The uncontrolled flooding of the Klivazh facility, which was designed to remain dry, could
520 cause anthropogenic radionuclides to contaminate groundwater and the wider geological
521 environment and lead to human exposure to radiation. A looming environmental catastrophe
522 could be virtually impossible to control, driven by the amplifying power of winds, water

523 flows, and the interconnectedness of mines (Yakovliev & Chumachenko, 2017). The active
524 migration of contaminants in the direction of the drainage basin of the Siverskyi Donets, as
525 well as rivers flowing into the Sea of Azov (e.g. the Krynka and Mius), highlight that this is
526 of international significance (Chumachenko & Yakovliev, 2017) (Fig. 6).

527 Surface deformation data over the Donetsk and Luhansk oblasts reveal that other areas of
528 Donbas are undergoing rebound, such as the Pervomaysk mining district in Luhansk (Ulytsky
529 *et al.*, 2018; Ministry of Ecology and Natural Resources of Ukraine, 2019) (Fig. 6). Heave is
530 also identified in the surrounds of the city of Donetsk, over areas known to be mined, and is
531 identified nearby to concentric and often high-rate areas of subsidence. Similar deformations
532 are detected elsewhere across the oblasts, particularly notable in central Donetsk and southern
533 Luhansk. Implementing such a modelling approach as applied to Horlivka would likely
534 provide beneficial information to the Ukrainian authorities as well as to environmental,
535 diplomacy and intergovernmental organizations. The data highlights the ‘hidden’
536 environmental degradation that is occurring and such information could help to avoid a
537 potential ecological disaster. A monitoring service could be implemented in near real-time
538 with the aid of the Sentinel-1 mission. This could provide updates as frequently as every six
539 days and could also be of use to assist in remediation efforts once the conflict is resolved.

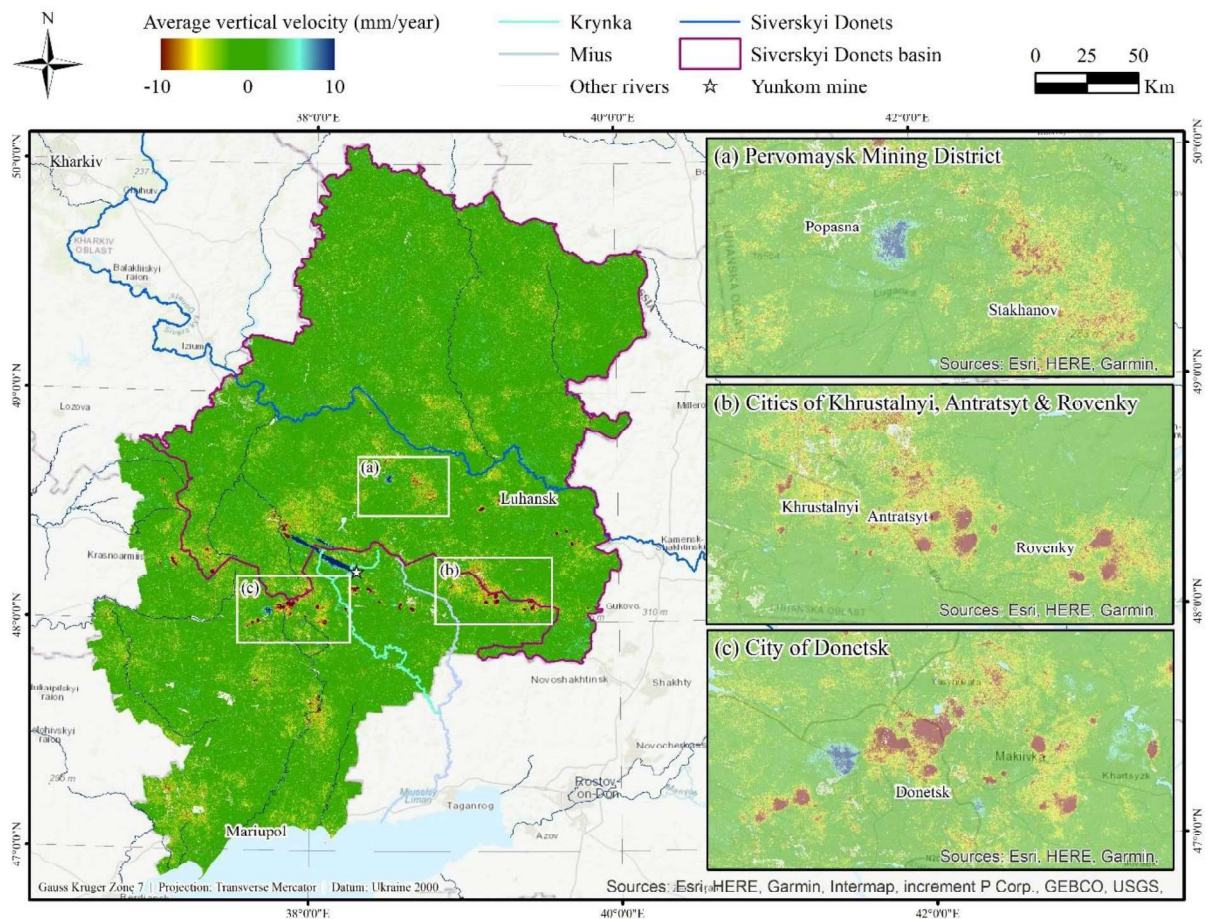
540

541

542

543

544



545

546 **Figure 6.** Surface deformation over the Donetsk and Luhansk oblasts with rivers (Polczynski, 2018) and the
 547 Siverskyi Donets drainage basin (Ministry of Ecology and Natural Resources of Ukraine, 2019) (within Donetsk
 548 and Luhansk only) overlaid. The river Krynka includes the tributaries of the Korsunka and Bulavina.

549

550

551 **6. Conclusion**

552 Identifying the rise of minewater in recently abandoned coalfields is challenging because
 553 ground measurements are often spatio-temporally sparse or not available at all. Obtaining
 554 adequate information on when and where minewater might surface are vital to avoid
 555 detrimental consequences following coalfield abandonment. The method presented in this
 556 study, based upon satellite radar interferometry, provides a remote, non-invasive solution to

557 spatio-temporally monitor and forecast the rise of minewater which could be implemented in
558 near-real time. The application to Horlivka identified that potentially radioactive minewater
559 within the Yunkom mine could reach the level of the natural water table by the middle of
560 2024. This approach is highly advantageous in isolated or inaccessible areas, such as Donbas,
561 where there is an urgent need to assess the hydrodynamic state of the mines due to the
562 possibility of the spread radioactive contaminants, but no possibility of carrying out a
563 comprehensive *in-situ* analysis.

564

565

566

567 **References**

568 Adams, R., and Younger, P.L., 1997, Simulation of groundwater rebound in abandoned
569 mines using a physically based modelling approach. In: Veselic, M., and Norton, P.J.
570 (editors) *Proceedings of the 6th International Mine Water Association Congress, "Minewater
571 and the Environment"*, Bled, Slovenia, 8 - 12th September 1997. Volume 2: 353 - 362.

572 Alsaab, D., Elie, M., Izart, A., Sachsenhofer, R.F., Privalov, V.A., Suarez-Ruiz, I., Martinez,
573 L. and Panova, E.A., 2009. Distribution of thermogenic methane in Carboniferous coal seams
574 of the Donets Basin (Ukraine): "Applications to exploitation of methane and forecast of
575 mining hazards". *International Journal of Coal Geology*, 78, pp. 27-37.

576 <https://doi.org/10.1016/j.coal.2008.09.004>

577 Bekendam, R.F. and Pöttgens, J.J., 1995. Ground movements over the coal mines of
578 southern Limburg, The Netherlands, and their relation to rising mine waters. *Land
579 Subsidence (Proc. Fifth Int. Symp. On Land Subsidence, The Hague, October 1995)*. IAHS
580 Publ. no. 234., pp.3-12.

581 Béjar-Pizarro, M., Ezquerro, P., Herrera, G., Tomás, R., Guardiola-Albert, C., Hernández,
582 J.M.R., Merodo, J.A.F., Marchamalo, M. and Martínez, R., 2017. Mapping groundwater level
583 and aquifer storage variations from InSAR measurements in the Madrid aquifer, Central
584 Spain. *Journal of Hydrology*, 547, pp.678-689. <https://doi.org/10.1016/j.jhydrol.2017.02.011>

585 Boni, R., Cigna, F., Bricker, S., Meisina, C. and McCormack, H., 2016. Characterisation of
586 hydraulic head changes and aquifer properties in the London Basin using Persistent Scatterer
587 Interferometry ground motion data. *Journal of Hydrology*, 540, pp.835-849.
588 <https://doi.org/10.1016/j.jhydrol.2016.06.068>

589 Castellazzi, P., Longuevergne, L., Martel, R., Rivera, A., Brouard, C. and Chaussard, E.,
590 2018. Quantitative mapping of groundwater depletion at the water management scale using a
591 combined GRACE/InSAR approach. *Remote Sensing of Environment*, 205, pp.408-418.
592 <https://doi.org/10.1016/j.rse.2017.11.025>

593 Castellazzi, P., Martel, R., Rivera, A., Huang, J., Pavlic, G., Calderhead, A.I., Chaussard, E.,
594 Garfias, J. and Salas, J., 2016. Groundwater depletion in Central Mexico: Use of GRACE and
595 InSAR to support water resources management. *Water Resources Research*, 52(8), pp.5985-
596 6003. <https://doi.org/10.1002/2015WR018211>

597 Chen, J., Chen, J., Liao, A., Cao, X., Chen, L., Chen, X., He, C., Han, G., Peng, S., Lu, M.
598 and Zhang, W., 2015. Global land cover mapping at 30 m resolution: A POK-based
599 operational approach. *ISPRS Journal of Photogrammetry and Remote Sensing*, 103, pp.7-27.
600 <https://doi.org/10.1016/j.isprsjprs.2014.09.002>

601 Chumachenko S.M., and Yakovliev Y.O, 2017. Hazardous gas-geochemical contamination of
602 geological environment from the horlivka chemical plant. *Journal of the Chromatographic*
603 *Society – V. XVII.* – P. 16-26. Available at: <
604 http://zht.igns.gov.ua/journal/JRN_2017/PDF/5.PDF> [Accessed 4th March 2022]

605 Crosetto, M., Solari, L., Mróz, M., Balasis-Levinsen, J., Casagli, N., Frei, M., Oyen, A.,
606 Moldestad, D.A., Bateson, L., Guerrieri, L. and Comerci, V., 2020. The evolution of wide-
607 area DInSAR: From regional and national services to the European Ground Motion Service.
608 *Remote Sensing*, 12(12), p.2043. <https://doi.org/10.3390/rs12122043>

609 Cuenca, M.C., Hooper, A.J. and Hanssen, R.F., 2013. Surface deformation induced by water
610 influx in the abandoned coal mines in Limburg, The Netherlands observed by satellite radar
611 interferometry. *Journal of Applied Geophysics*, 88, pp.1-11.
612 <https://doi.org/10.1016/j.jappgeo.2012.10.003>

613 Donabedov, A.T., 1940. On study of the physical properties of rocks from coal-bearing
614 basins of the USSR. *Sov. geologiya*, (7), pp.77-85.

615 Dudek, M., Tajduś, K., Misa, R. and Sroka, A., 2020. Predicting of land surface uplift caused
616 by the flooding of underground coal mines—A case study. *International Journal of Rock*
617 *Mechanics and Mining Sciences*, 132, p.104377.
618 <https://doi.org/10.1016/j.ijrmms.2020.104377>

619 Eastern Option, 2020. *Ecological catastrophe in Enakievo. Mine waters poison rivers and*
620 *stakes. Eastern Option*. [online]. Available at :<[https://v-](https://variant.com.ua/article/kolohycheskaia-katastrofa-v-enakievo-shakhtn-e-vod-otravlaiut-reky-y-stavky/)
621 [variant.com.ua/article/kolohycheskaia-katastrofa-v-enakievo-shakhtn-e-vod-otravlaiut-reky-](https://variant.com.ua/article/kolohycheskaia-katastrofa-v-enakievo-shakhtn-e-vod-otravlaiut-reky-y-stavky/)
622 [y-stavky/>](https://variant.com.ua/article/kolohycheskaia-katastrofa-v-enakievo-shakhtn-e-vod-otravlaiut-reky-y-stavky/) [Accessed 1st April 2022].

623 Gee, D., Bateson, L., Grebby, S., Novellino, A., Sowter, A., Wyatt, L., Marsh, S.,
624 Morgenstern, R. and Athab, A., 2020. Modelling groundwater rebound in recently abandoned
625 coalfields using DInSAR. *Remote Sensing of Environment*, 249, p.112021.
626 <https://doi.org/10.1016/j.rse.2020.112021>

627 Gee, D., Bateson, L., Sowter, A., Grebby, S., Novellino, A., Cigna, F., Marsh, S., Banton, C.
628 and Wyatt, L., 2017. Ground motion in areas of abandoned mining: application of the

629 Intermittent SBAS (ISBAS) to the Northumberland and Durham Coalfield, UK. *Geosciences*,
630 7(3), p.85. <https://doi.org/10.3390/geosciences7030085>

631 Gee, D., Sowter, A., Grebby, S., de Lange, G., Athab, A. and Marsh, S., 2019. National
632 geohazards mapping in Europe: Interferometric analysis of the Netherlands. *Engineering*
633 *Geology*, 256, pp.1-22. <https://doi.org/10.1016/j.enggeo.2019.02.020>

634 German Aerospace Center., 2018. *TanDEM-X - Digital Elevation Model (DEM) - Global*,
635 *90m*. <https://doi.org/10.15489/ju28hc7pui09>

636 Hamm, V., Collon-Drouaillet, P. and Fabriol, R., 2008. Two modelling approaches to water-
637 quality simulation in a flooded iron-ore mine (Saizerais, Lorraine, France): A semi-
638 distributed chemical reactor model and a physically based distributed reactive transport pipe
639 network model. *Journal of contaminant hydrology*, 96(1-4), pp.97-112.
640 <https://doi.org/10.1016/j.jconhyd.2007.10.004>

641 Hoffmann, J., Zebker, H.A., Galloway, D.L. and Amelung, F., 2001. Seasonal subsidence and
642 rebound in Las Vegas Valley, Nevada, observed by synthetic aperture radar interferometry.
643 *Water Resources Research*, 37(6), pp.1551-1566. <https://doi.org/10.1029/2000WR900404>

644 Hook, K. and Marcantonio, R., 2022. Environmental dimensions of conflict and paralyzed
645 responses: the ongoing case of Ukraine and future implications for urban warfare. *Small Wars*
646 *& Insurgencies*, pp.1-29. <https://doi.org/10.1080/09592318.2022.2035098>

647 Malinowska, A.A., Witkowski, W.T., Guzy, A. and Hejmanowski, R., 2020. Satellite-based
648 monitoring and modeling of ground movements caused by water rebound. *Remote Sensing*,
649 12(11), p.1786. <https://doi.org/10.3390/rs12111786>

650 Ministry of Ecology and Natural Resources of Ukraine, 2019. *State of the Siverskyi Donets*
651 *Basin and Related Risks under Military Operations. Technical Report*. Organization for

652 Security and Co-operation in Europe, Vienna, Austria. Available at:<
653 <https://www.osce.org/files/f/documents/8/6/419459.pdf>> [Accessed 1st April 2022]

654 Poland, J.F., 1984. *Guidebook to studies of land subsidence due to ground-water withdrawal*.
655 UNESCO, Paris, France.

656 Polczynski, M., 2018, *Base Maps of Ukraine – Rivers*.
657 <https://doi.org/10.7910/DVN/8D3WSO>

658 Privalov, V.A., Zhykalyak, M.V. and Panova, E.A., 2003. Geologic controls on coalbed
659 occurrence in the Donets Basin (Ukraine). *Proceedings of the 3rd International Methane and*
660 *Nitrous Oxide Mitigation Conference*, Beijing, China, 17-21 November 2003.

661 Sachsenhofer, R.F., Privalov, V.A., Zhykalyak, M.V., Bueker, C., Panova, E.A., Rainer, T.,
662 Shymanovskyy, V.A. and Stephenson, R., 2002. The Donets Basin (Ukraine/Russia):
663 coalification and thermal history. *International Journal of Coal Geology*, 49, pp. 33-55.
664 [https://doi.org/10.1016/S0166-5162\(01\)00063-5](https://doi.org/10.1016/S0166-5162(01)00063-5)

665 Sachsenhofer, R.F., Privalov, V.A. and Panova, E.A., 2012. Basin evolution and coal geology
666 of the Donets Basin (Ukraine, Russia): An overview. *International Journal of Coal Geology*,
667 89, pp. 26-40. <https://doi.org/10.1016/j.coal.2011.05.002>

668 Sadovenko, I., Ulytsky, O., Zahrytsenko, A. and Boiko, K., 2020. Risk assessment of
669 radionuclide contamination spreading while flooding coal mined-out rocks. *Mining of*
670 *Mineral Deposits*, 14(4), pp.130-136. <https://doi.org/10.33271/mining14.04.130>

671 Samsonov, S., d'Oreye, N. and Smets, B., 2013. Ground deformation associated with post-
672 mining activity at the French–German border revealed by novel InSAR time series method.
673 *International Journal of Applied Earth Observation and Geoinformation*, 23, pp.142-154.
674 <https://doi.org/10.1016/j.jag.2012.12.008>

675 Sherwood, J.M., and Younger, P.L., 1997, Modelling groundwater rebound after coalfield
676 closure. In: Chilton, P.J., et al, (editors), *Groundwater in the urban environment, Volume 1:
677 Problems, processes and management*. A.A. Balkema Publishers, Rotterdam. 165 - 170.

678 Sowter, A., Athab, A., Novellino, A., Grebby, S. and Gee, D., 2018. Supporting energy
679 regulation by monitoring land motion on a regional and national scale: A case study of
680 Scotland. *Proceedings of the Institution of Mechanical Engineers, Part A: Journal of Power
681 and Energy*, 232(1), pp.85-99. <https://doi.org/10.1177/0957650917737225>

682 Sowter, A., Amat, M.B.C., Cigna, F., Marsh, S., Athab, A. and Alshammari, L., 2016.
683 Mexico City land subsidence in 2014–2015 with Sentinel-1 IW TOPS: Results using the
684 Intermittent SBAS (ISBAS) technique. *International Journal of Applied Earth Observation
685 and Geoinformation*, 52, pp.230-242. <https://doi.org/10.1016/j.jag.2016.06.015>

686 Sowter, A., Bateson, L., Strange, P., Ambrose, K. and Syafiudin, M.F., 2013. DInSAR
687 estimation of land motion using intermittent coherence with application to the South
688 Derbyshire and Leicestershire coalfields. *Remote Sensing Letters*, 4(10), pp.979-987.
689 <https://doi.org/10.1080/2150704X.2013.823673>

690 Surinaidu, L., Rao, V.G., Rao, N.S. and Srinu, S., 2014. Hydrogeological and groundwater
691 modeling studies to estimate the groundwater inflows into the coal Mines at different mine
692 development stages using MODFLOW, Andhra Pradesh, India. *Water Resources and
693 Industry*, 7, pp.49-65. <https://doi.org/10.1016/j.wri.2014.10.002>

694 State Ecological Academy postgraduate education and Department of the Ministry of
695 Ecology and natural resources of Ukraine, 2018. *Statement Results Report Ecological
696 Situation On Donetsk And Territories Luhansk Region*. Kyiv, Ukraine. Available at:<
697 <http://dea.edu.ua/img/source/Doc/LugDon%20Obl.pdf>> [Accessed 1st April 2022]

698 Stovba, S.M. and Stephenson, R.A., 1991. The Donbas Foldbelt: its relationships with the
699 uninverted Donets segment of the Dniepr–Donets Basin, Ukraine. *Tectonophysics*, 313, pp.
700 59-83. [https://doi.org/10.1016/S0040-1951\(99\)00190-0](https://doi.org/10.1016/S0040-1951(99)00190-0)

701 Terzaghi, K., 1925. Principles of soil mechanics, IV—Settlement and consolidation of clay.
702 *Engineering News-Record*, 95(3), pp.874-878.

703 Todd, F., McDermott, C., Harris, A.F., Bond, A. and Gilfillan, S., 2019. Coupled hydraulic
704 and mechanical model of surface uplift due to mine water rebound: implications for mine
705 water heating and cooling schemes. *Scottish Journal of Geology*, 55(2), pp.124-133.
706 <https://doi.org/10.1144/sjg2018-028>

707 Torres, R., Snoeij, P., Geudtner, D., Bibby, D., Davidson, M., Attema, E., Potin, P.,
708 Rommen, B., Floury, N., Brown, M. and Traver, I.N., 2012. GMES Sentinel-1 mission.
709 *Remote sensing of environment*, 120, pp.9-24. <https://doi.org/10.1016/j.rse.2011.05.028>

710 Ulytsky, O., Yermakov, V., Lunova, O. and Buglak, O., 2018. Environmental risks and
711 assessment of the hydrodynamic situation in the mines of Donetsk and Lugansk regions of
712 Ukraine. *Journal of Geology, Geography and Geoecology*, 27(2), pp.368-376.
713 <https://doi:10.15421/111861>

714 Yakovliev, Y., Chumachenko, S., Morsch, Y., Romanyuk, V. and Nikitin, A., 2020. Potential
715 radiation impact of the burial of the “Klivazh” facility on the Yunkom mine. *Political Science
716 and Security Studies Journal*, 1(2), pp.98-106. <https://doi.org/10.5281/zenodo.4538369>

717 Yakovliev, Y. and Chumachenko, S., 2017. Ecological Threats in Donbas, Ukraine. *Centre
718 for Humanitarian Dialogue. Geneva*, 64. Available at: <[https://ceobs.org/wp-](https://ceobs.org/wp-content/uploads/2020/04/Ecological-Threats-in-Donbas.pdf)
719 [content/uploads/2020/04/Ecological-Threats-in-Donbas.pdf](https://ceobs.org/wp-content/uploads/2020/04/Ecological-Threats-in-Donbas.pdf) > [Accessed 4th March 2022]

720 Yermakov, V., Lunova, O. and Averin, D., 2019. Potential territorial risk in eastern Ukraine.
721 *Journal of Geology, Geography and Geoecology*, 28(3), pp.600-609.
722 <https://doi.org/10.15421/111957>

723 Younger, P.L., 2016. A simple, low-cost approach to predicting the hydrogeological
724 consequences of coalfield closure as a basis for best practice in long-term management.
725 *International Journal of Coal Geology*, 164, pp.25-34.
726 <https://doi.org/10.1016/j.coal.2016.06.002>

727 Younger, P.L. and Adams, R., 1999. *Predicting mine water rebound*. Environment Agency
728 *R&D Technical Report W179*. Bristol, UK. 108pp.

729 Yu, M.H., Jefferson, I.F. and Culshaw, M.G., 2007. Fault reactivation, an example of
730 environmental impacts of groundwater rising on urban area due to previous mining activities.
731 In *The Second Half Century of Rock Mechanics, Three Volume Set: 11th Congress of the*
732 *International Society for Rock Mechanics*, 3 VOLUMES+ CD-ROM (Vol. 1, p. 41). CRC
733 Press.

734 Zhao, J. and Konietzky, H., 2020. Numerical analysis and prediction of ground surface
735 movement induced by coal mining and subsequent groundwater flooding. *International*
736 *Journal of Coal Geology*, 229, p.103565. <https://doi.org/10.1016/j.coal.2020.103565>

737 Zhao, J. and Konietzky, H., 2021. An overview on flooding induced uplift for abandoned coal
738 mines. *International Journal of Rock Mechanics and Mining Sciences*, 148, p.104955.
739 <https://doi.org/10.1016/j.ijrmms.2021.104955>

740

741 **Acknowledgements**

742 This work was funded by Terra Motion Limited. Sentinel-1 SAR data was provided by the
743 European Space Agency and mining and hydrogeological data by the State Ecological
744 Academy of Postgraduate Education and Management, Ukraine. The authors would like to
745 thank five anonymous reviewers and the Science of the Total Environment editorial team
746 who helped to improve the quality of the manuscript

747

748 **Author Contributions**

749 A.A., D.G., Z.W., and A.S. contributed to the InSAR processing. D.G. devised the modelling
750 framework and performed the groundwater analysis. All of the authors participated in the
751 data interpretation. D.G. led the writing of the manuscript where all of the authors contributed
752 and participated in manuscript editing and final approval.

753

754 **Declaration of Competing Interest**

755 The authors declare no conflicts of interest.

756

757 **Data Availability**

758 Data is available from the corresponding author on reasonable request.